TUDelft

Delft University of Technology

Postseismic coastal development in Aceh, Indonesia

Field observations and numerical modeling

Monecke, Katrin; Meilianda, Ella; Walstra, Dirk Jan; Hill, Emma M.; McAdoo, Brian G.; Qiu, Qiang; Storms, Joep E.A.; Masputri, Aisha Sri; Mayasari, Cut Deasy; Nasir, Muhammad

Important note
To cite this publication, please use the final published version (if applicable).
Please check the document version above.

Postseismic Coastal Development in Aceh, Indonesia -

Field Observations and Numerical Modeling

Katrin Monecke[1], Ella Meilianda[2], Dirk-Jan Walstra[3], Emma M. Hill[4], Brian G. McAdoo[5], Qiang Qiu[4,6], Joep Storms[7], Aisha Sri Masputri[8], Cut Deasy Mayasari[9], Muhammad Nasir[9], Indra Riandi[9], Agus Setiawan[8], Caroline Templeton[1]

[1] Wellesley College, 106 Central Street, Wellesley, MA 02481, USA

[2] Tsunami and Disaster Mitigation Research Center (TDMRC), Syiah Kuala University, Banda Aceh,

Indonesia

[3] Deltares, Delft, The Netherlands

[4] Earth Observatory of Singapore / Asian School of the Environment, Nanyang Technological University,

Singapore

[5] Yale-NUS College, Singapore

[6] University of Leeds, United Kingdom

[7] Delft University of Technology, Delft, The Netherlands

[8] Department of Civil Engineering, Syiah Kuala University, Banda Aceh, Indonesia

[9] Department of Civil Engineering, Teuku Umar University, Meulaboh, Indonesia

Abstract

We model postseismic changes to the shoreline of West Aceh, Indonesia, a region largely affected by the December 2004 Sumatra-Andaman earthquake and ensuing Indian Ocean tsunami, using a cross-shore morphodynamic model. Subsidence of 0.5 – 1.0 m and tsunami scouring during the 2004 event caused the complete destruction of the beach and the landward displacement of the western coast of Aceh by an average of 110 m. Comparing a series of satellite images and topographic surveys, we reconstruct the build-up of a new beach ridge along a 6 km long stretch of coastline in the years following the event. We then use the cross-shore model UNIBEST-TC developed for a wave-dominated sandy shoreline to determine the controlling factors of shoreline recovery. Input parameters include bathymetric data measured in 2015, grain size characteristics of offshore sediment samples, modeled wave data, tidal elevations from a nearby tide-gauge station as well as measured and modeled postseismic uplift data. After establishing a cross-shore profile in equilibrium with the prevailing hydrodynamic conditions, we

simulate the post-tsunami recovery, the effect of the monsoon seasons, as well as the influence of postseismic land level changes for up to 10 years and compare them to the observed coastal development. Our modeling results indicate that the recovery of the western Acehnese shoreline after the 2004 tsunami was quick with littoral sediment transport normalizing to pre-tsunami conditions within two to four years following the event. However, field data shows that the shoreline stabilized 50-90 m landward of its pre-2004 tsunami position, most likely due to the build-up of a prominent higher beach ridge in response to coseismic subsidence. Observed variability in shoreline position in the order of a few tens of meters since 2009 can be attributed to seasonal wave climate variability related to the monsoon cycle. The effect of postseismic uplift on shoreline position is small and in the order of only a few meters over 10 years, which is 3 to 5 times smaller than long-term coastal progradation rates that are driven by abundant sediment supply to the littoral zone. This overall progradational trend will promote preservation of seismically modified beach ridges, which can serve as paleoseismic indicators.

Keywords

Coastal Hazards, Beach Ridge Morphology, Coastal Modeling, Paleoseismology, 2004 Indian Ocean Tsunami, Aceh (Indonesia)

1. Introduction

The effect of extreme events on coastline morphology has been surveyed in the immediate aftermath of large storms and tsunamis along coastlines around the world. These observations allow scientists to determine hydrological conditions such as storm surge patterns (e.g., Fritz et al. 2007, Spencer et al. 2014), tsunami wave heights and inundation distances (e.g., Jaffe et al. 2006) as well as geomorphic change and sediment transport (e.g., Tappin et al. 2012; Vargas et al. 2011). Characterizing these processes will help to prepare vulnerable shorelines for future hazards. Understanding not only the impact but also the recovery of shorelines after extreme events is important as coastal planners, charged with the rebuilding of the coastline, have to allocate resources accordingly. Post-event beach surveys as well as satellite image analysis usually cover the time span of a few months to a couple of years and have shown that the onset of regular coastal processes and the recovery of shorelines can be quick (Wang et al. 2006, Liew et al. 2010). While some shorelines grow back to their original positions (e.g., Choowong et al. 2009) other shorelines might be affected on longer time scales depending on the prevailing wave energy (Yu et al. 2013), complexities related to seismically induced land level changes (Meilianda et al. 2010) or the availability of sand due to drastic land use changes in the drainages feeding the littoral zone (McAdoo and Paravisini, 2011). Recently it has been postulated that an understanding of long-term coastal evolution over decades and centuries within a larger coastal framework is crucial in addressing current coastal management problems (e.g., Stive et al. 2002; Cowell et al. 2003).

Sustainable coastal management also requires knowledge of how frequently a shoreline is hit by coastal hazards such as tsunamis and how large these might be. While more commonly deposits in coastal marshlands have been analyzed to reconstruct large-scale overwash events, in a few cases coastal

morphology of sandy shorelines has been used to identify past seismic events. For instance, Wells and Goff (2007) correlate the formation of coastal dune ridges with the mobilization of sediment during earthquakes along the Alpine Fault in New Zealand. Nelson and Manley (1992) identify prominent beach ridges within an elevated strandplain on Mocha Island, Chile, that could potentially mark rapid earthquake-induced uplift events. Erosional escarpments within a beach ridge plain on Kenai Peninsula in Alaska are interpreted to form during coseismic subsidence and landward erosion during Alaskan megathrust earthquakes (Kelsey et al. 2015). Monecke et al. (2015) describe the formation of a higher beach ridge in response to coseismic subsidence and higher relative sea levels in the aftermath of earthquakes along the Sunda trench. However, the preservation potential of seismically modified coastal morphologies remains unclear.

Coastal models provide a powerful tool to understand the controlling factors of coastal morphologies and to forecast shoreline evolution. Process-based coastal models that simulate sediment transport and morphological change in response to the prevailing hydrodynamic conditions (i.e., currents and waves) have been capable of predicting coastal development for a range of time and spatial scales. Studies include the evolution of single beach sites over weeks, months and years (e.g. Ruessink et al. 2007; Ruggiero et al. 2009; Walstra et al. 2012, 2016) or of entire tidal basins over millennia (e.g. Van der Wegen and Roelvink 2008). While more often applied to evaluate the effect of coastal engineering practices such as beach nourishments, process-based models have also been successfully used to understand the impact of coastal hazards such as sea level rise (e.g., Aagard and Sørensen 2012), storms (e.g., Roelvink et al. 2009) and tsunami inundation (e.g., Apostos et al. 2011).

In this study, we build on previous investigations in West Aceh, Indonesia, that quantified shoreline change since the 2004 Sumatra-Andaman earthquake using satellite imagery and repetitive beach surveys (Monecke et al. 2015). We apply the cross-shore model UNIBEST – TC (Ruessink et al. 2007; Walstra et al. 2012) to new field data collected in West Aceh in 2015 including beach surveys, bathymetric data and sediment samples. Hydrodynamic boundary conditions are simulated using measured tidal elevations and modeled wave data. Post-seismic land level changes are inferred from a nearby permanent GPS station and viscoelastic mantle relaxation models. Based on these model inputs, we first analyze the controlling factors of shoreline recovery after the complete destruction of the beach during the Sumatra-Andaman earthquake and ensuing Indian Ocean tsunami. We then investigate shoreline variability as observed on satellite images and field surveys since 2004 and explore the effect of postseismic uplift on coastal morphology.

2. Study site

2.1. Seismotectonic setting

The southwest coast of Aceh, the northernmost province of Sumatra Island, Indonesia, runs parallel to the Sunda trench, where the Indian-Australian and Sunda plates converge at a rate of ~53 mm/y (Figure 1a). The northern part of this plate boundary ruptured last in the great M=9.2 December 2004 Sumatra-Andaman earthquake over a length of 1600 km, with slip locally exceeding 20 m (Chlieh et al. 2007). The

resulting vertical displacement of the seafloor caused a tsunami that devastated shorelines in the Indian Ocean region. Significant land level changes occurred in a wide region of southeast Asia, with the southwest coast of Aceh experiencing coseismic subsidence of 0.5 – 1.0 m (Meltzner et al. 2006; Subarya et al. 2006). Since late 2005, postseismic land level changes have been recorded by the permanent GPS station Ujong Muloh, UMLH, of the Sumatra GPS Array, SuGAR, (Figure 1a) and indicate uplift of ~2.7 cm/y along the southwest coast of Aceh. This uplift is likely a result of viscoelastic mantle relaxation following the earthquake (Gunawan et al. 2014). Modeled postseismic vertical displacements at our study site taking into account afterslip from all recent events and viscoelastic mantle flow following the two largest events, the 2004 Sumatra-Andaman and the 2005 Nias earthquakes (Figure 1a), suggest exponential decay with initial uplift rates of 4.4 cm/y in early 2005 decreasing to 1.4 cm/y and less since mid-2006 (Qui et al. 2016). This is an approximation of a most likely more complicated curve.

2.2 Coastal geomorphology

The study site is located 15 km northwest of Meulaboh, the district capital of West Aceh (Figure 1a). This region is situated within the Meulaboh embayment, a low lying area southwest of the Barisan Mountains, which run the length of Sumatra (Cameron et al. 1983). Several hundred meter thick fluvial to paralic sediments that are associated with nearshore coral reef deposits were laid down here since the Pliocene. Widespread fluvial terraces along major rivers that dissect the Meulaboh Embayment from northeast to southwest, as well as raised coral reefs and a prograding coastline point towards long-term uplift in this area (Cameron et al. 1983). Combined with substantial weathering rates under a tropical climate we can assume large sediment supply from rivers to the littoral zone.

Our investigations focus on a 6 km long stretch of coastline between the Woyla River in the northwest and a raised coral reef structure to the southeast (Figure 1b). This coastal area is characterized by beach ridge morpohologies that can be traced at least 2 km inland before dense swamp vegetation obscures the terrain. Beach ridges run parallel to the coast and mark former positions of a prograding coastline. They curve towards the raised coral reef structure in the southeast and become wider and less well-pronounced near the Woyla river floodplain (Figure 1b). Shore-normal creeks and man-made channels periodically cut through the ridges. Beach ridge crests are no higher than 2.8 m above mean sea level and sandy ridges are separated by low-lying swales that are often flooded and accumulate peaty muds. Radiocarbon dates obtained from such peaty deposits indicate long-term coastal progradation of 1.3-1.8 m per year over the last 1000 years (Monecke et al. 2008, 2015).
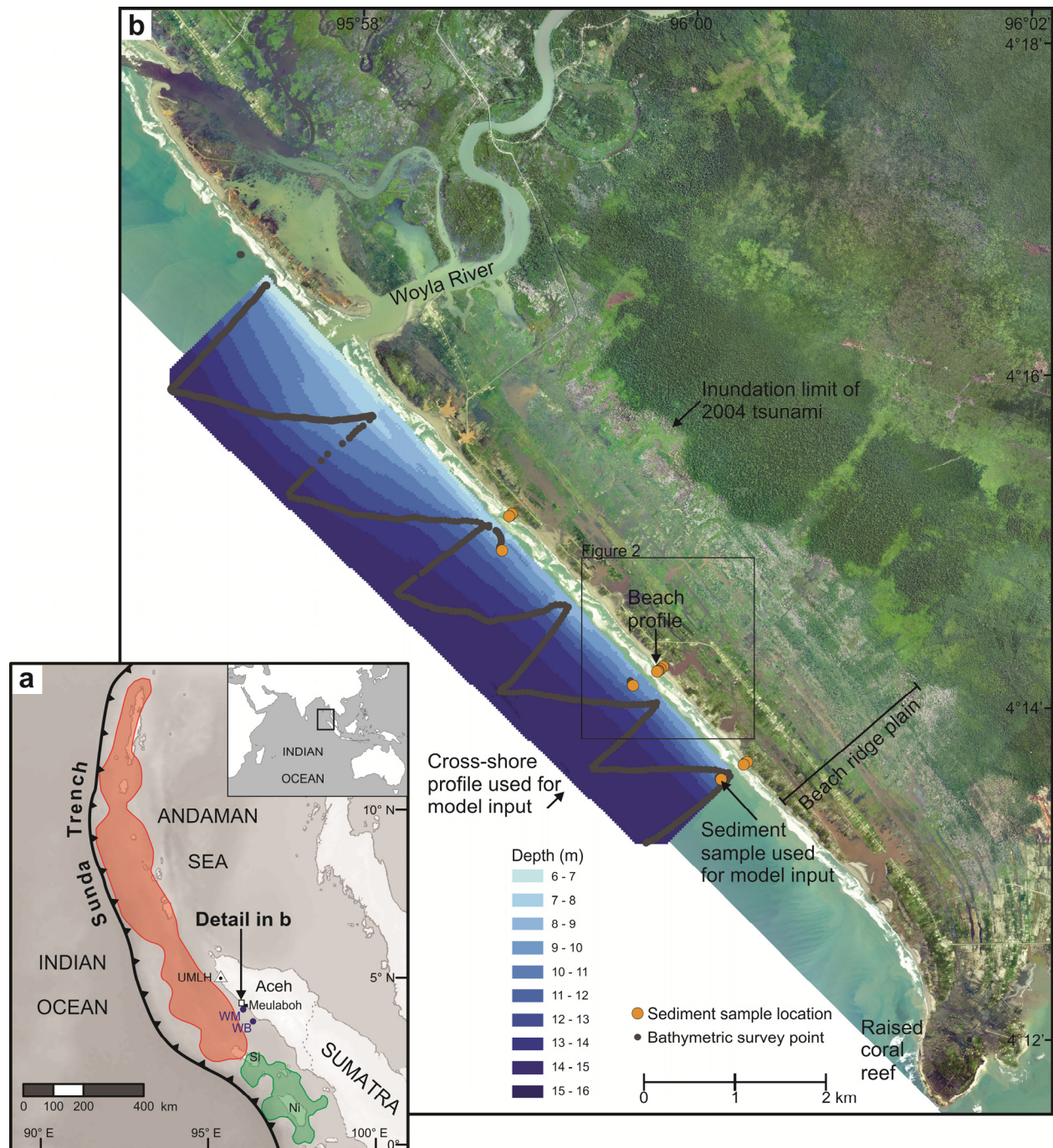
Figure 1: Overview of study area. a) Tectonic setting. Red and green patches mark rupture areas of 2004 Sumatra- Andaman earthquake (after Chlieh et al. 2007) and 2005 Nias-Simeulue earthquake (after Konca et al. 2007), respectively. Triangle marks permanent GPS station Ujong Muloh, UMLH, of the Sumatra GPS Array, SuGAR. Blue dots indicate location of wave buoy (WB) and modeled wave data (WM). Si is Simeulue island, Ni is Nias Island. b) Overview of beach ridge plain and bathymetric map with survey and sediment sample locations. Aerial photograph is from April 2005 and made available by the SIM Center of the Aceh and Nias Rehabilitation and Reconstruction Board (BRR). Inundation limit of 2004 tsunami is boundary between saltwater-affected vegetation in grey and healthy vegetation in green. Note large scours along coastline and flooding of swales within beach ridge plain. Notice coastal road and village on prominent beach ridge in ~640 m distance to shore.

The coastline of West Aceh is shaped by a strong swell with the wave climate being controlled by the East Monsoon from ~ November to April and the more energetic West Monsoon from ~ May to October, which comes with rougher seas and more frequent storms. Waves approach the coast predominantly from a southwesterly direction and reach maximum wave heights of H_s = 1.75 m during the East Monsoon and up to H_s = 2.25 meters during the West Monsoon (de Graaff 2007). Semidiurnal tidal variations are minor with a tidal range of 0.5 – 0.6 m measured at a nearby tidal gauge in Meulaboh during spring tides (University of Hawaii Sea Level Center, UHSLC, Caldwell et al. 2015). The beach profile is relatively steep with an average foreshore gradient of 0.07. Surface sediments along the beach profile are composed of well sorted medium sand consisting of siliciclastic particles and less frequent heavy minerals.

Tsunami wave heights of 9-14 m in 2004 (Kongko et al. 2006) and inundation distances of between 2 and 2.5 km, as visible in Figure 1b, devastated the shoreline of West Aceh. Satellite images taken before and 3 days after the December 2004 earthquake indicate the complete destruction of a wide sandy beach ridge along this coastline (Liew et al. 2010). Subsequent satellite images show the rapid but incomplete rebuilding of a new prominent beach ridge in the years following the earthquake (Figure 2; Liew et al. 2010, Monecke et al. 2015) which is bound by a swale and a permanently vegetated area at its landward edge (Figures 1b and 2). Local residents report that overwash during storm events can affect the entire ridge and reach close to the vegetated area. In 2006, we were able to analyze the internal structure of the newly forming ridge in a man-made trench and observe low-angle cross-stratification and heavy mineral laminations, thus indicating that it is probably formed by swash processes in combination with occasional overwash events. We didn't observe any dune growth on top of the ridges, possibly because of disruptive energetic overwash events and widespread coastal swamp vegetation. Onshore sediment transport results in the regular closing of shore-normal creeks and channels (Figure 2) and residents periodically re-open pathways by hand or with heavy machinery to avoid flooding of inland areas. However, often the openings close again within days or weeks posing considerable challenges for residents.

3. Field site data acquisition

To quantify coastal retreat in West Aceh in December 2004 and progradation since then, Monecke et al. (2015) traced shorelines on six sets of aerial photographs and satellite imagery along an 18 km long stretch of coastline including our study site and covering both monsoon seasons from the years 2002 – 2013. Details of this analysis are given in Monecke et al. (2015).

We repeatedly measured a shore-normal transect along a central path of the beach ridge plain using an automatic level suitable for a remote and densely vegetated environment and allowing height, distance and angle readings (Figure 3, for location see Figures 1b and 2). We cross-checked distances between surveyed points with a range finder and hand-held GPS. While the 2009, 2012, and 2013 transects extended 1850 m, 680 m and 710 m inland, we surveyed only the modern beach ridge in 2015. Because of the lack of benchmarks in our area, we used sea level as our vertical reference, which was corrected

for the tidal excursion as measured at the Meulaboh tide gauge station. The position of the coastal road in 640 m distance to shore and the deepest point of the most seaward swale serve as horizontal reference points. Maximum horizontal positioning errors in our surveys comprise measurement and instrument errors detected when cross-checking points using Geographic Information Systems (GIS) software (Table 1). Vertical offsets include instrument and measurement errors that are relatively minor in our surveys (Table 1). However, we have to account for a large vertical error when interpreting sea level since wave set-up can cause significant displacement of water up the dry beach especially during higher energetic conditions. As a rule of thumb, wave set-up is given as 20% of the offshore significant wave height (Masselink and Hughes, 2011). Using the maximum wave heights of H_s = 1.75 m for surveys during the East Monsoon and H_s = 2.25 m during the West Monsoon, errors in sea level - and therefore for all elevations on our transects - amount to 0.35 m and 0.45 m, respectively (Table 1).

Since no high resolution nautical charts are available for our study site, we conducted a bathymetric survey in 2015 using a simple depth sounder operated from a local fishing boat, following a zigzag pattern (Figure 1b). Due to intense wave shoaling and breaking in the nearshore zone the boat could not get closer than ~300 m to shore. We corrected recorded depth data for tidal variations for the duration of the survey. We then created a bathymetric map by interpolating between surveyed points using ArcGIS software (Figure 1b).

We collected sediment surface samples along the measured beach profile and further to the south and north to capture alongshore variability (Figure 1 b). Three grab samples from the sea floor were obtained in about 10 m water depth at three locations along the investigated coastal stretch (Figure 1b). We cleaned the samples of any plant debris and sieved to < 1000 microns before measuring them using a Beckman-Coulter laser diffraction particle size analyzer.

4. Shoreline change observations

Spatial imagery analysis revealed co- and postseismic shoreline changes in West Aceh that were quantified by Monecke et al. (2015) and are only summarized here. Reported shoreline positions depend on the season when the image was taken, and carry uncertainties of up to ±16.4 m related to hydrodynamic variations and minor errors in the digitizing process. A minimum average shoreline retreat of 110 m was measured along the surveyed 18 km long stretch of the Acehnese coastline due to subsidence and tsunami scouring in 2004, with erosion being largest at the mouths of natural creeks and drainage channels (Monecke et al. 2015, compare Figures 2a and 2b). Within the first 4 months following the earthquake a narrow beach had formed (Figure 2b). Between April 2005 and June 2006 the coastline advanced rapidly by an average of 22 m corresponding to a progradation rate of ~ 18 m/yr. It then advanced more slowly by an additional 30 m between mid-2006 and the end of 2009. April 2011 imagery that coincides with the late phase of the East Monsoon, shows only minor shoreline accretion of 5 m compared to 2009 and marks the furthest seaward position since the 2004 tsunami (Figure 2c); however, at this point the shoreline was still about 50 m landward of its pre-2004 position. Most recent satellite images available to us from June 2013 in the middle of the West Monsoon season, indicate a

renewed retreat of an average 41 m (Figure 2d) thus, placing the shoreline in vicinity of the June 2006 shoreline and on average about 90 m landward of its pre-tsunami position.

Figure 2: Detail of Figure 1b showing pre-tsunami conditions (i.e. 2002) and post tsunami coastal development. Red line marks 2002 shore in all images. Triangles indicate location of beach surveys (see Figure 3) and mark top of beach ridge and most seaward swale in 2015. April 2005 and 2011 images were taken towards the end of the East Monsoon season; 2002 and 2013 images during the more energetic West Monsoon. Satellite imagery is from *Quickbird* (2002), *World-View-2* (2011) and *Pleiades* (2013). 2005 aerial photographs are from the SIM Center of the Aceh and Nias Rehabilitation and Reconstruction Board (BRR).

Shore-normal topographic surveys reveal alternating ridges and swales and an overall low morphology with maximum elevations not exceeding 2.8 m above sea level (or 4.6 m above the Meulaboh tide gauge reference level, Figure 3). The most seaward ridge that formed in the aftermath of the 2004 earthquake, is the most prominent one in the sequence of beach ridges with widths between 110 - 163 m and crests 1.1 - 2.8 m above sea level (or 2.9 – 4.6 m above the Meulaboh tide gauge reference level) depending on the time of survey. It shows a typical asymmetric shape with a steep seaward face and a more gently sloping landward face. The crest of this newly built beach ridge is 0.8 – 1.3 m higher than ridges further inland. Comparison of the four beach transects has to be done with care since sea level, our vertical reference point, is poorly constrained due to variations in wave set-up. While there is little change to the landward facing side of the beach ridge, shoreline positions vary by up to 49 m with the coast being located further seaward during the East Monsoon and further landward during the more energetic West Monsoon. The beach ridge is exposed to a variable extent depending on the wave conditions during the time of survey and foreshore slopes fluctuate between 0.04 and 0.11 with steeper slopes in later years.
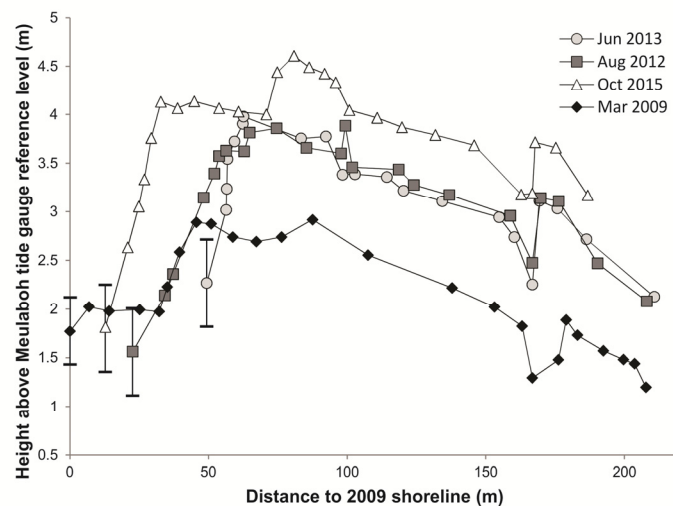

Figure 3: Results of automatic level surveys for years 2009, 2012, 2013 and 2015. Most seaward point in each transect represents sea level at the time of survey, which is corrected for the tidal elevation as recorded at the Meulaboh tide gauge station but includes error due to variable wave set-up (see table 1). Note the variability in shoreline position of up to 49 m especially between surveys conducted in the midst of the East Monsoon (2009) versus the West Monsoon (2012, 2013). Prominent beach ridge forming in the aftermath of the 2004 earthquake extends from the coastline to a swale in ~ 160 m distance to the shore.

Date of survey	Horizontal Error	Vertical Error			
	Measurement and instrument error (m)	Instrument error (m)	Measurement error (m)	Wave set-up (m)	RMS error (m)
3/10/2009	5	0.0007	0.1	0.35	0.36
8/31/2012	10	0.002	0.02	0.45	0.45
6/12/2013	15	0.002	0.005	0.45	0.45
10/6/2015	2.5	0.002	0.02	0.45	0.45

Table 1: Error related to topographic surveys shown in Figure 3. RMS is root mean square error. Surveys are referenced to sea level, which can vary due to wave set-up. Wave set-up is estimated as 20% of the maximum offshore significant wave height for the respective monsoon seasons after Masselink and Hughes (2011).

5. Coastal modeling

5.1 The coastal model UNIBEST-TC

In order to determine the controlling factors of the observed shoreline changes in West Aceh and forecast coastal development in response to postseismic land level changes, we applied the coastal model UNIBEST-TC (Ruessink et al. 2007, Walstra et al. 2012) to our field data. The model is designed to compute sediment transport and resulting sea bed changes along a sandy cross-shore profile in response to the prevailing hydrodynamic conditions, over time scales that range from hours to years. The UNIBEST-TC model has successfully been used to study the dynamics of cross-shore profiles that are influenced by seasonal wave climate variability, or modified by beach nourishments and sand extractions (e.g., see references in Walstra 2000). Model runs start with the input of an initial cross-shore profile and time series of seasonally averaged representative wave conditions from offshore. Computations of wave propagation and energy dissipation will feed into equations describing nearshore currents, which in turn will be used to determine sediment transport and bed level changes. Computed bottom changes will be applied in the next time step, thus providing a coupled model of sea bed evolution.

5.2 Model input parameters

5.2.1 Boundary conditions

Annual wave data from 2007 to 2013 recorded at an offshore buoy in 4.5 km distance to the shoreline and located ~70 km to the southeast of our study area (Figure 1a) indicate two major directions of wave approach: west to west-southwest and south to south-southeast, with the latter being more prevalent. Wave heights range mostly between 0.5 - 1.5 m but can reach up to 2.5 m. The wave climate at this location is probably influenced by waves passing between Simeulue and Nias Islands (Figure 1a) leading to a wave field with a strong southerly component. Additional seasonal wave data for the west coast of Aceh comes from modeled wave data by de Graaff (2007), who used the wave model SWAN (Simulating Waves Nearshore) and offshore wind and wave data from the European Centre for Medium-Range Weather Forecast (ECMWF). Computed for a nearshore location (approximately 8 m water depth) close to Meulaboh (Figure 1a), this model shows wave approach from the southwest with significant wave heights of H_s = 0.75 – 1.25 and rare occurrences of waves up to H_s = 1.75 m during the East Monsoon. Significant wave heights during the more energetic West Monsoon lie between H_s = 0.75 – 1.75 m but can occasionally be as high as H_s = 2.25 m. Dominant peak wave periods range from T_p = 10 - 14 seconds. For model input, we base our wave data on the wave climate model by de Graaff (2007), since it is in good agreement with the measured data and is calculated for a location closer to our study site. Furthermore, it discriminates between the monsoon seasons and includes information on wave period, an essential parameter in the model formulations. Relative percentages of the angles of wave approach, significant wave heights with a resolution of 0.5 m and peak wave periods for each monsoon season were translated into a year-long time series with half day intervals of a specific combination of wave angle, height and period. We accounted for storm events by grouping larger wave heights of up to H_s=

1.5 m during the East Monsoon and H_s = 2.0 m during the West Monsoon throughout the time series (Figure 4a). For final input into the model we converted significant wave heights to root mean square wave heights (H_{rms}) as required by the model. To test the sensitivity of the model we varied wave heights by $\pm$10% (Supplementary Figure 1). Cross-shore profile evolution is similar for all scenarios with larger wave heights causing increased offshore sediment transport resulting in a slightly wider active profile.

A tide gauge station in Meulaboh installed in 2008 as part of Indonesia's Tsunami Early Warning System (Figure 1a, Schöne et al. 2011), indicates a microtidal environment with a semidiurnal tide and a maximum tidal range of 0.5 - 0.6 m during spring tides. We use quality-controlled data from November 2009 to October 2010 made available for this station by the University of Hawaii Sea Level Center (UHSLC, Caldwell et al. 2015) to build a year-long time series with hourly intervals of water level elevations (Figure 4b).
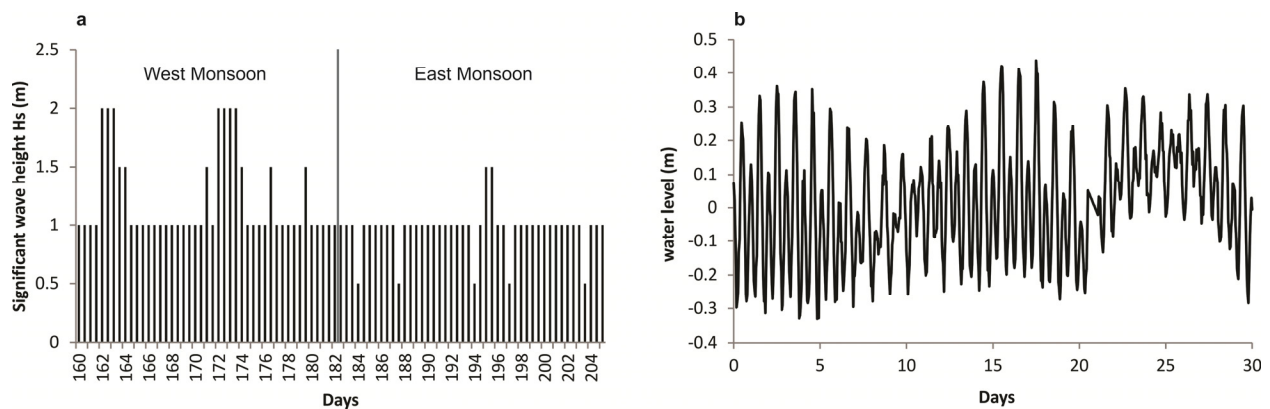

Figure 4: Visualization of boundary conditions. a) Partial time series of wave heights with resolution of 0.5 m based on wave model by de Graaff (2007) and averaged for half day intervals with higher-energetic conditions and more frequent storms during the West Monsoon. Horizontal axis values are days since the start of the West Monsoon. b) Partial time series of water level elevations based on hourly quality controlled data from the tide gauge station in Meulaboh made available by the University of Hawaii Sea Level Center (UHSLC), Caldwell et al. (2015).

A cross-shore profile has to be developed that serves as the initial sea bed in model runs (Figure 5). As a base we use bathymetric and topographic data obtained in October 2015 (Figures 1b and 3). We closed the data gap in the energetic nearshore zone, and smoothed the profile using a polynomial fit. We then extended the profile inland to avoid model instabilities (Figure 5). After running the model under the prevailing hydrodynamic conditions for 1 year, the shoreline gets displaced landward and the profile develops a nearshore bar in 2 – 3 m water depth, which is a common feature in surf zone morphology (Masselink and Hughes, 2011). The bar is most likely formed due to sediment convergence of the onshore directed transport related to wave asymmetry and the offshore directed undertow. The last cross-shore profile after a 1 year run can be assumed to be in equilibrium with the local hydrodynamic processes and is used as the starting profile in future runs. For model runs investigating the immediate

shoreline recovery after tsunami inundation, we modify the equilibrium profile using post-tsunami bathymetric survey data from North Aceh by Jaffe et al. (2006) and explained later in the text.
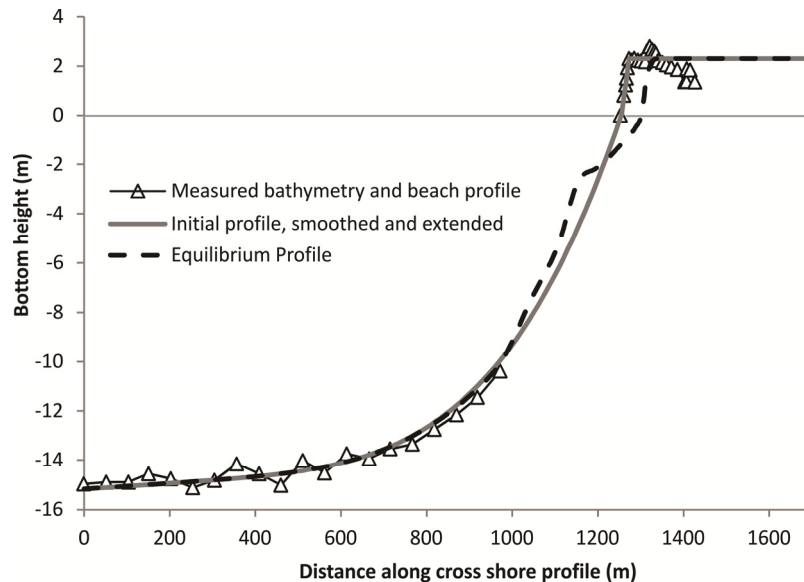

Figure 5: Development of equilibrium profile. Initial profile (gray) is based on bathymetry and beach profile as measured in 2015 (triangles, see Figures 1b and 2 for locations) but smoothed and extended further landward. Equilibrium profile (black dashed line) represents the last bottom profile developing from the initial profile under prevailing hydrodynamic conditions during a one-year run.

Sediment samples collected along the beach and in the upper surf zone are composed of well-sorted medium sand (Figure 6). Grain size distributions of offshore samples collected in about 10 m water depth (Figure 1b) show a large variability of moderately sorted fine, medium and coarse sand probably related to changing energy conditions in a cross-shore direction and varying distances to the Woyla river that carries a high suspension load. D_{50} and D_{90} values of 213 μm and 404 μm, respectively, matching the intermediate grain size distribution of offshore samples, were chosen for model input. Because of the difficulties to measure the grain size of suspended sediment, we estimated it as 80% of the D_{50} value of the bed load (170 μm), which is an acceptable approximation (van Rijn, 1987). We used a cross-shore varying grain size with grain sizes increasing by a factor of 1.67 towards shore. We tested the sensitivity of the model to grain size variation by varying grain size by ± 10% (Supplementary Figure 2). We observed a response similar to the wave height sensitivity analysis with parallel evolution of the cross-shore profiles for all scenarios with finer grain sizes being slightly more susceptible to offshore sediment transport resulting in a wider active profile.
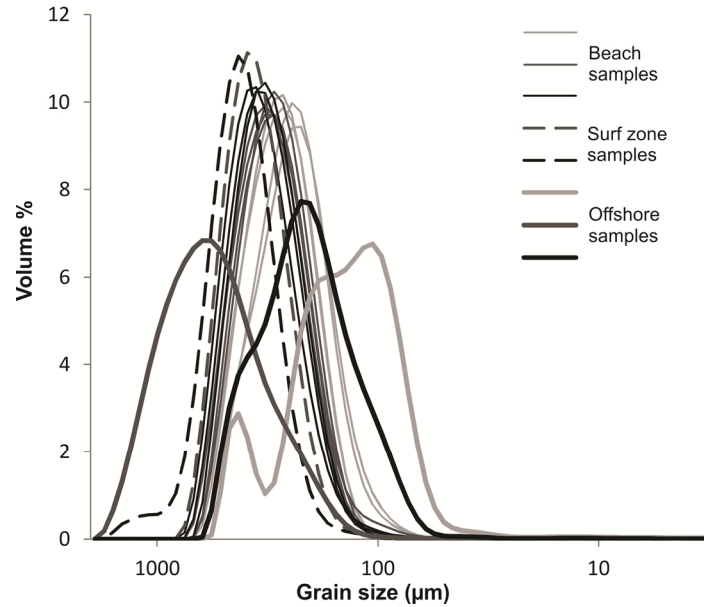
Figure 6: Grain size distributions of sediment samples collected along three beach transects and offshore (see Figure 1b for sampling locations). Hairlines mark beach samples, dashed lines are for upper surf zone samples and thick solid lines for offshore samples. Darker gray tones indicate increasing distance to the Woyla River of sampled transects. Note the better sorting of beach and surf zone samples in contrast to offshore samples as well as coarser grain sizes with increasing distance from the Woyla River. Notice the high variability of offshore samples. Statistics of the intermediate grain size distribution of offshore samples were used for input into the model (black thick solid line).

5.2.2 Run and model parameters

We varied the grid size along the cross-shore profile from 80 m in the deepest part to only 4 m in the upper part of the profile above ~ 6 m water depth, where changes to the profile are larger and more rapid. Since the model is not designed to capture morphodynamic changes in the very shallow inner surf zone, calculations are stopped in some depth and transport is extrapolated from the last wet computational point to the dry beach. Depending on the incident wave period our computations stop in 1.6 – 3.0 m water depth. Simulations were carried out at a time step of 1.5 hours with output generated once per day. Only bed level changes of up to 5 cm in 14.4 minutes were allowed before a smaller time step was used to overcome run instabilities. Wave-, current- and transport specific run parameters were adjusted within the range of acceptable values to best fit the measured bathymetry and foreshore slope and to mirror the steep and reflective nature of the shoreline.

6. Modeling results

6.1 Shoreline recovery after the December 2004 earthquake and tsunami

First, we designed model runs to understand the extent and time frame of shoreline recovery after large-scale scouring during tsunami inundation in 2004. We modified the initially developed equilibrium

profile and built a cross-shore profile that reflects immediate post-tsunami conditions. These are inferred from field observations by the International Tsunami Survey Team (ITST) measuring bathymetry in an area about 100 km to the North of our study area in April 2005 and November 2007 (personal communications with Peter Ruggiero, University of Oregon, and Guy Gelfenbaum, United States Geological Survey (USGS); Jaffe et al. 2006). The shoreface here is somewhat shallower than in our study area but experiences similar wave climates with a strong southwesterly swell (de Graaff 2007) and was subjected to comparable tsunami wave heights in excess of 15 m (Jaffe et al. 2006). The April 2005 bathymetric profile shows the remnants of an offshore bar in 12-13 m water depth that was completely reworked in November 2007. Apostos et al. (2011) model sediment transport during tsunami inundation along this same profile and show that the largest erosion occurs close to shore with sediment being transported offshore by the backwash of the tsunami. Deposition of eroded material takes place in 7-14 m water depth in form of a sandbar. Additional model runs with varying shoreface morphology by Apostos et al. (2011) indicate that a steeper profile would cause erosion over a smaller distance and deposition in a narrower sand bar located closer to shore. Taking these observations into account we built an erosional post-tsunami cross-shore profile for our study site with 110 m landward displacement of the shore, as observed in satellite images, and a prominent offshore bar in 7 – 14 m water depth, while maintaining the overall foreshore and shoreface slopes along the profile (Figure 7a). We then start a 10-year run beginning with wave conditions corresponding to December 26, the day of tsunami inundation, in the midst of the less energetic East Monsoon season.

Model runs show a nearly complete reworking of the offshore bar over the time span of a few years (Figure 7a). Regular wave processes cause sediment from the sand bar to be rapidly moved up the profile causing an upward shift of the shoreface and coastline progradation thus, nearly restoring the equilibrium profile and presumable pre-tsunami conditions. Coastal progradation rates are in the order of ~15 m/yr over the first four years and slow to < 5 m/yr in years 6-10 of the model run. The model allows us to plot sediment transport rates at each point along the cross-shore profile (Figure 7b). For a position corresponding to the top of the sand bar in 920 m cross-shore distance, daily onshore sediment transport rates are two to four times higher for the post-tsunami profile compared to transport from the same location in the equilibrium profile in the first ~ 4 years. For both profiles, onshore sediment transport is largest during higher-energetic conditions, i.e. during the West Monsoon season and during storm events (Figure 7b). Overall sediment transport rates for the equilibrium profile remain constant from year to year, while transport along the post-tsunami profile decreases with time and slowly approaches the same equilibrium conditions. After 10 years the post-tsunami profile still shows a small residual sand bar below 12 m depth (Figure 7a) and sediment transport rates remain slightly above those of the equilibrium profile (Figure 7b).
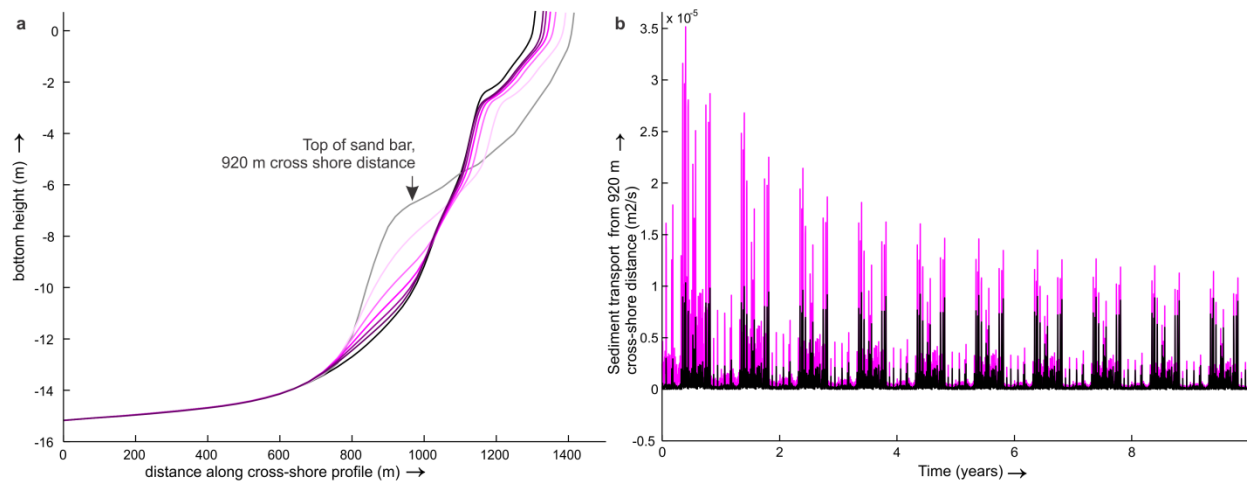
Figure 7: Modeling results of shoreline recovery after tsunami inundation. a) Evolution of cross-shore profile. Black profile is the equilibrium profile. Gray profile is reconstructed post-tsunami cross-shore morphology showing landward displaced shoreline and prominent offshore sandbar that formed from backwash of the tsunami. Pink profiles are post-tsunami profiles after 2, 4, 6, 8 and 10 years with darker shades indicating later years. Note the quick reworking of sandbar and shoreline progradation in early years. b) Total sediment transport rates from top of sandbar in 920 m cross shore distance of post-tsunami profile over 10 years (pink) relative to sediment transport from same location for equilibrium profile (black). Individual columns represent one day and positive values indicate onshore transport. Note that sediment transport rates remain constant for the equilibrium profile over 10 years while up to four times larger transport rates occur in the sandbar profile especially in earlier years. For both profiles higher transport rates correlate with higher energetic wave conditions during storms and the West Monsoon.

6.2 Seasonal variations

In order to study the effect of the monsoon seasons on coastal morphology we used the initially developed equilibrium profile and applied the hydrodynamic conditions repeating in a 1 year loop over a time span of 10 years. We then compare the two cross-shore profiles representing the last day of the West and East Monsoon for each year (Figure 8).

We observe significant profile changes and a large exchange of sediment between the foreshore and an offshore bar between seasons. During the more energetic West Monsoon an erosional profile develops with the shoreline being displaced approximately 20 m landward (Figure 8). In addition, the profile is lowered and a ~100 m wide and ~2 m high bar forms in 4-8 m water depth. During calmer wave conditions for the duration of the East Monsoon, sediment from the offshore bar is brought back to shore, the coastline progrades and the bar is reduced in width and height and moves upward along the profile to shallower water depths. An overall accretionary trend develops in our profiles over multiyear runs (Figure 8). In order isolate the effect of postseismic land level changes, this trend has to be subtracted from future model runs.
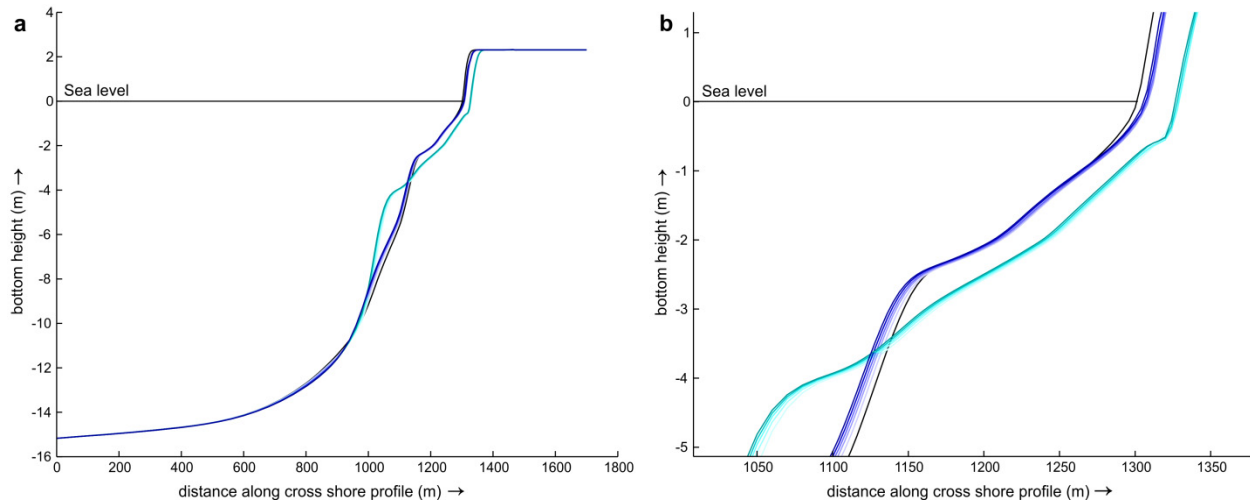
Figure 8: Cross-shore profile evolution over five years under prevailing hydrodynamic conditions showing the large effect of the monsoon seasons on the profile and on shoreline position. Black profile is the equilibrium profile, blue profiles are after the East Monsoon and turquoise profiles are after the more energetic West Monsoon. Darker shades indicate later years. a) Overview. b) Detail. Note the slight accretionary trend over five years, which is a modeling effect.

6.3 The effect of postseismic land level changes

Next we studied the effect of shoreline change in response to rapid postseismic uplift measured at the permanent GPS station north of our study area and suggested in viscoelastic mantle relaxation models. We repeated our tidal elevation series for 10 years and adjusted for relative sea level fall and, for comparison relative sea level rise, at each time step. We use constant land level change rates of 2.7 cm/y as measured by the permanent GPS station as well as modeled rates with exponentially decaying postseismic uplift showing initial rates of 4.4 cm/y and 1.4 cm/y and lower after ~1.5 years. We simulate each of the sea level scenarios for ten years and then subtract the slight accretionary trend observed in our earlier stable sea level runs to isolate the effect of changing sea levels on the cross-shore profile.

With the land rising and relative sea level dropping 27 cm in 10 years, we observe a downward shift of the cross-shore profile by roughly the same amount as sea level change (Figure 9). Erosion occurs across the upper shoreface and accretion below a water depth of 3 m. The shoreline shows a small seaward shift in the order of a few meters over 10 years or at a rate of ~0.4 m/yr. More energetic conditions during the West Monsoon affect the profile in the same way but at deeper depths; i.e. erosion occurs down to 7 m water depth with sediment being deposited below this depth. Relative sea level rise has the opposite effect on the cross-shore profile: Sediment is moved towards shore from below water depths of 3 m during the East Monsoon and from below 7 m during the West Monsoon, resulting in an upward shift of the cross-shore profile and a slight landward displacement of the shore of a few meters in 10 years. When simulating exponentially decaying sea level change rates, changes to the cross-shore profile are minimally larger until about year 3 and then become much less compared to model runs with a constant rate of sea level change.
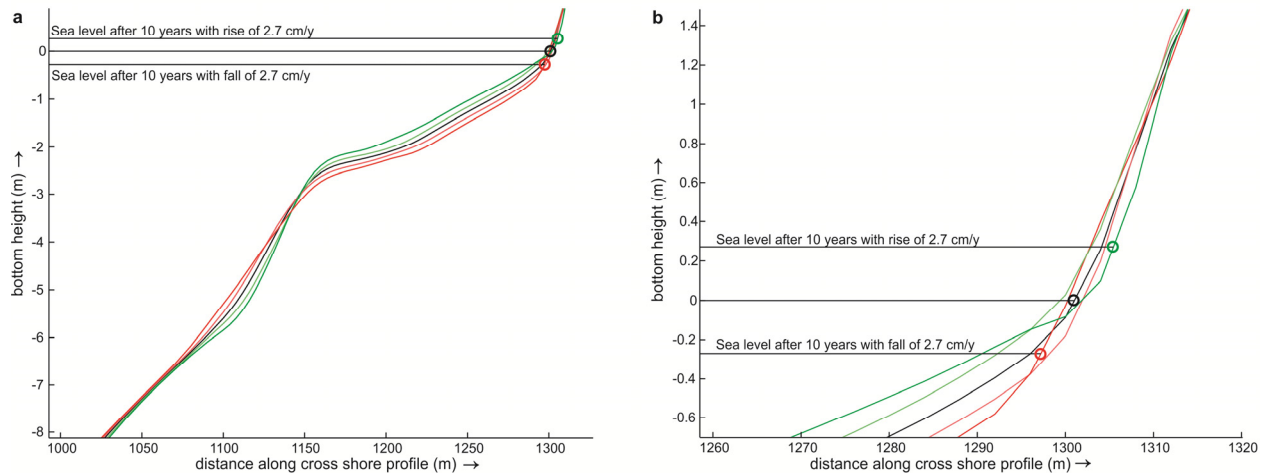
16

Figure 9: Model results showing the effect of relative sea level fall (red) and rise (green) on the cross shore profile and shoreline position. a) Overview. b) Detail. Black profile is the equilibrium profile. Lighter red and green shades represent profiles after 5 years, darker shades after 10 years. Note the lowering of the upper shoreface and seaward displacement of the shore during sea level fall and opposite response during sea level rise.

7. Discussion

Liew et al. (2010) describe the quick rebuilding of a narrow beach in West Aceh within 13 months following the 2004 event. Beach accretion slowed down in the following years and probably reached some equilibrium between 2006 and 2009 as seen in more recent spatial imagery (Figure 2). Our modeling results match the observed rapid coastal progradation and suggest that coastal recovery in West Aceh was very quick and mostly completed within 2- 4 years after tsunami inundation. The reworking of sand transported offshore by the backwash of the tsunami seems to be the most likely source for post-tsunami coastal progradation. The recovery of beaches after extreme events depends on the magnitude of the event, the inherited hydrodynamic conditions, sediment availability and the considered time scales. After 90 days of post-storm recovery on the US Gulf of Mexico coast, Wang et al. (2006) observe complete restoration of berm height following erosion from Hurricane Ivan but a more landward location of the shoreline in the order of a few 10s of meter possibly because of loss of sediment due to aeolian transport. Yu et al. (2013) note rapid and complete restoration of a high-energy Hong Kong beach within a few months following Typhoon Hagupit, whereas little post-storm change occurred along a low-energy beach. This matches our model results for West Aceh with highly energetic conditions during the West Monsoon being more efficient in transporting sediment back to shore (Figure 7b). Along tsunami-affected coastlines, Tappin et al. (2012) noticed the quick infilling of breaches and channels along the Sendai coastline in Japan within days of tsunami scouring in 2011. Morton et al. (2008) suggest that sediment transported offshore in Sri Lanka by the backwash of the 2004 tsunami was brought back to shore within weeks. In Thailand, Choowang et al. (2009) measure the almost complete recovery of the shoreline position over only two years after a retreat of ~ 25 m in December 2004, however, this coastline was not affected by coseismic land level changes.

While the post-tsunami recovery in West Aceh is most likely completed, the shoreline is located several tens of meters landward of its pre-tsunami position, likely as a combination of large-scale coseismic subsidence and loss of sediment during tsunami inundation. The new beach ridge that formed after complete destruction of the beach in 2004, stands out 0.8 – 1.3 m higher than beach ridges further inland (Figure 3). This is interpreted as a result of coseismic subsidence, where a higher relative sea level will cause swash processes to act at a higher level, thus causing the build-up of a ridge at a higher elevation with the available sand filling additional accommodation space created by subsidence (Monecke et al., 2015). Furthermore, numerous scours were formed along the coast during 2004 tsunami inundation, which were filled rapidly within the first few months after the earthquake (Figure 2). Some sediment might have also been moved into depths not reached by regular wave processes over multi-year scales and therefore, been at least temporarily lost from the coastal system. In addition, a considerable amount of sand was transported as far as 1.8 km inland forming a tsunami sand sheet in the coastal marshes (Monecke et al., 2008). Similar to West Aceh, Meilianda et al. (2010) found incomplete recovery of a beach in northwest Aceh, with only 60% of the initial sand volume restored as well as ongoing erosion along another beach after the first six months following 2004 tsunami inundation. Here, a less energetic wave climate as well as the presence of offshore troughs associated with the Sumatran Fault probably cause sediment to be lost from the coastal system over much longer time scales.

After formation of the prominent ~160 m wide beach ridge in the months and early years following the earthquake, variations in shoreline position of up to 49 m were observed on satellite images and during beach surveys in West Aceh since 2009 with shorelines being located further landward during the more energetic West Monsoon (Figures 2 and 3). We didn't notice any major changes in shoreline orientation between the two monsoon seasons, thus indicating that measured shoreline retreat or advance is a result of cross-shore rather than along-shore adjustments to the seasonally changing wave climate. Our modeling results suggest that changes in the order of a few tens of meters can be caused by seasonal wave climate variability with shoreline positions during the West Monsoon being located further landward compared to shorelines during the East Monsoon (Figure 8). While we cannot reproduce the exact shoreline change most likely because of discrepancies between the used wave data and true wave conditions, the model matches the order of observed seasonal changes quite well. Such strong shoreline variability due to seasonal wave climate variations or periodic storm events is typical for other coastlines as well. Higher-energetic conditions lead to beach erosion and offshore sediment transport, whereas calmer wave conditions result in onshore sediment transport and beach accretion often with re-establishment of the same shoreline positions (Masselink and Hughes 2011). Depending on the strength of the seasonal cycle, the amount of shoreline change can be large and in the order of a few 10s of meter (e.g., Stive et al. 2002) similar to what we observe for the west coast of Aceh.

Postseismic land level changes in West Aceh are rapid and were expected to have an effect on coastal morphology over the next few decades. Our modeling results suggest that relative sea level changes cause a vertical shift of the cross-shore profile and a horizontal displacement of the coastline in the order of only a few meters over a decade or at a rate of ~0.4 m/yr, while the general shape of the profile is maintained (Figure 9). During initial model runs we developed an equilibrium profile that can be

assumed to be in balance with the prevailing hydrodynamic conditions especially sediment size and wave parameters (e.g., Dean 1987). Adjustments of the equilibrium profile when modeling different sea level scenarios, are due to sediment being carried towards shore during sea level rise and away from shore during sea level fall. This profile response probably reflects the shifting balance between onshore directed sediment transport due to wave asymmetry and offshore-directed transport due to the undertow (Roelvink and Stive 1990). Aargaard and Sørensen (2012) show that sea level rise will cause waves to break further landward and thus causing the convergence point of onshore and offshore directed sediment transport being translated towards shore. Over much of the cross-shore profile sediment is hence transported from the lower to the upper shoreface. They note further that increased offshore transport resulting in profile erosion only occurs very close to shore matching our modeling results that show a small landward displacement of the shoreline during sea level rise (Figure 9). In contrast, during sea level fall, we would expect the offshore directed undertow to extend further seaward. Sediment is transferred from the upper to the lower shoreface causing a lowering of the cross-shore profile similar to our model runs (Figure 9). We strictly consider only cross-shore profile changes in our model, even though it has been recognized that alongshore sediment distribution can play a major role in coastlines adjusting to sea level changes (e.g., Dean and Houston, 2016).

Considering much longer time scales in the order of centuries and millennia is essential in characterizing many coastal systems (Cowell et al. 2003). Long-term shoreline evolution is a function of sediment supply, the steepness of the shoreface, eustatic sea level change and relative sea level variations caused by sediment loading, compaction and tectonic adjustments (e.g., Helland-Hansen and Hampton, 2009). The coastline in West Aceh experienced long-term coastal progradation of 1.3-1.8 m per year over the last 1000 years as evidenced by the sequence of beach ridges extending at least 2 km inland (Fig. 1b; Monecke et al. 2008, 2015). This rate is 3 to 5 times higher than shoreline advance predicted as a result of postseismic land level changes in our model runs. Therefore, shoreline progradation and beach ridge growth in West Aceh is most likely dominated by a continuous large supply of sediment to the littoral zone from an actively deforming hinterland under a tropical climate. Similarly, sediment supply has been found to be the most important factor in creating beach ridge plains around the world since the stabilization of sea levels in the mid-Holocene (e.g. Bristow and Pucillo 2006, Anthony 1995). Relative sea level fall due to postseismic uplift in West Aceh will add to the general progradational trend but will only have a minor effect on the long-term coastal development especially since the rate of viscoelastic mantle relaxation is expected to decrease and cease after a few decades (Shearer and Buergmann 2010).

The overall progradational trend of the coastline is favorable for preservation of the prominent higher beach ridge forming in response to coseismic subsidence in the aftermath of the 2004 earthquake. Earlier topographic surveys extending further inland found an additional pronounced beach ridge in about 640 m distance to the shore that is partially occupied by the coastal road and village (Figure 1b, Monecke et al. 2015). Based on its stratigraphic position within the beach ridge plain, this prominent ridge has been interpreted to have formed in the aftermath of the last great subduction earthquake (Monecke et al. 2015) that caused significant land-level changes close to Simeulue Island in the mid-15th century (Figure 1a, Meltzner et al. 2010). It is also matching sedimentary records from the same beach

ridge plain that found evidence of tsunami inundation shortly after AD 1290-1400 just landward of this prominent ridge (Monecke et al., 2008).While we have no evidence for pronounced beach ridges further inland due to limited accessibility, these initial results suggest that coseismically altered beach ridges are preserved in West Aceh and can serve as paleoseismic indicators.

8. Conclusions

We measured shoreline changes to a beach ridge plain in West Aceh, Indonesia, since the 2004 Sumatra-Andaman earthquake and ensuing Indian Ocean tsunami on satellite images and in the field. We then successfully applied the cross-shore model UNIBEST-TC to the field data to simulate hydrodynamic conditions and to investigate the controlling factors of postseismic coastal development. Satellite images and topographic data indicate the quick rebuilding of a prominent ~160 m wide beach ridge since the nearly complete destruction of the beach in 2004. While not fully reestablishing its pre-2004 position, our modeling results suggest that the recovery of the coast and return to equilibrium conditions was rapid and most likely completed within 2-4 years after the tsunami. The formation of a higher beach ridge in response to coseismic subsidence and a higher relative sea level as well as sediment loss due to large-scale off- and onshore transport during tsunami inundation are the most likely causes for the shoreline stabilizing landward of its pre-2004 position. Coastline changes in the order of a few 10s of meters observed since 2009 can be simulated in coastal model runs and are interpreted as seasonal shoreline variations caused by changes in wave climate during alternating monsoon seasons. However, these seasonal changes are not large enough to cause significant modifications to the prominent new beach ridge. While coseismic subsidence left an imprint on coastal morphology in the form of a relatively higher beach ridge, modeling results suggest that the effect of postseismic uplift will be small and cause only a slight lowering and seaward shift of the cross-shore profile within the next few decades. Long-term coastal progradation rates that are 3-5 times larger than the effect of postseismic uplift and are driven by large sediment input to the littoral zone, will be more significant in future coastal development. Considering the long-term accretionary trend of the coastline in West Aceh, we suggest that coseismically altered beach ridge morphologies are preserved and can serve as paleoseismic indicators. We propose that in the near-field of other subduction zones capable of producing large ruptures with significant land level changes, coastal morphologies can give important clues in identifying past earthquakes and assessing the seismic hazard.

Acknowledgements

References

Aagaard, T., Sørensen, P., 2012. Coastal profile response to sea level rise: a process-based approach. Earth Surface Processes and Landforms 37, 354–362.

Anthony, E. J., 1995. Beach ridge development and sediment supply: examples from West Africa. Marine Geology 129, 175-186.

Apotsos, A., Gelfenbaum, G., Jaffe, B., 2011. Process‐based modeling of tsunami inundation and sediment transport. Journal of Geophysical Research 116, F01006, doi:10.1029/2010JF001797.

Bristow, C.S., Pucillo, K., 2006. Quantifying rates of coastal progradation from sediment volume using GPR and OSL: the Holocene fill of Guichen Bay, south-east South Australia. Sedimentology 53, 769–788.

Caldwell, P. C., Merrfield, M. A., Thompson, P. R., 2015. Sea level measured by tide gauges from global oceans — the Joint Archive for Sea Level Holdings (NCEI Accession 0019568), Version 5.5, *NOAA National Centers for Environmental Information*, Dataset, doi:10.7289/V5V40S7W.

Cameron, N., 1983. The geology of the Takengon quadrangle, Sumatra. Explanatory note and geological map 1:250'000.

Chlieh, M., Avouac, J. P., Hjorleifsdottir, V., Song, T. R. A., Ji, C., Sieh, K., Sladen, A., Hebert, H., Prawirodirdjo, L., Bock, Y., Galetzka, J., 2007. Coseismic Slip and Afterslip of the Great Mw 9.15 Sumatra-Andaman Earthquake of 2004. Bulletin of the Seismological Society of America 97, 1A, S152-S173.

Choowong, S., Phantuwongraj, T., Charoentitirar, V., Chutakositkanon, S., Yumuand, P., Charusiri, 2009. Beach recovery after 2004 Indian Ocean tsunami from Phang-nga, Thailand. Geomorphology 104, 134–142.

Cowell, P.J., Stive, M.J.F., Niedoroda, A.W., De Vriend, H.J., Swift, D.J.P., Kaminsky, G.M., Capobianco, M., 2003. The coastal-tract (part 1): a conceptual approach to aggregated modeling of low-order coastal change. Journal of Coastal Research 19 (4), 812–827.

Dean, R.G., 1987. Additional sediment input to the nearshore region. Shore and Beach 25 (3–4), 76–81.

Dean, R.G., Houston, J.R., 2016. Determining shoreline response to sea level rise. Coastal Engineering 114, 1–8.

Fritz, H. M., Blount, C., Sokoloski, R., Singleton, J., Fuggle, A., McAdoo, B. G., Moore, A. L., Grass, C., Tate, B., 2007. Hurricane Katrina storm surge distribution and field observations on the Mississippi Barrier Islands. Estuarine, Coastal and Shelf Science 74, 12-20.

Graaff, R. de, 2007. Initial Modelling of Hydraulic Conditions. Aceh and Nias Sea Defense, Flood Protection, Refuges and Early Warning Project, BRR Concept Note/INFRA 300GI: WL | Delft Hydraulics Report.

Gunawan, E., Sagiya, T., Ito, T., Kimata, F., Tabei, T., Ohta, Y., Meilano, I., Hasanuddin Z. A., Agustan, Nurdin, I., Sugiyanto, D., 2014. A comprehensive model of postseismic deformation of the 2004 Sumatra–Andaman earthquake deduced from GPS observations in northern Sumatra. Journal of Asian Earth Sciences 88, 218-229.

Helland-Hansen, W., Hampson, G.J., 2009. Trajectory analysis: concepts and applications. Basin Research 21, 454–483.

Jaffe, B.E., Dengler, L., Hidayat, R., Kingsley, E., Kongko, W., Lukijanto, Moore, A., Titov, V., Yulianto, E., Borrero, J.C., Prasetya, G.S., Peters, R., McAdoo, B., Gelfenbaum, G., Morton, R., Ruggiero, P., Higman, B., 2006. Northwest Sumatra and offshore islands field survey after the December 2004 Indian Ocean tsunami. Earthquake Spectra 22 (s3), 105-135.

Kelsey, H. M., Witter, R. C., Engelhart, S. E., Briggs, R., Nelson, A., Haeussler, P., Reide Corbett, D., 2015. Beach ridges as paleoseismic indicators of abrupt coastal subsidence during subduction zone earthquakes, and implications for Alaska-Aleutian subduction zone paleoseismology, southeast coast of the Kenai Peninsula, Alaska. Quaternary Science Reviews 113, 147-158.

Konca, A. O., Hjorleifsdottir, V., Song, T.-R. A., Avouac, J.-P., Helmberger, D. V., Ji, C., Sieh, K., Briggs, R., Meltzner, A., 2007. Rupture kinematics of the 2005 *Mw* 8.6 Nias-Simeulue earthquake from the joint inversion of seismic and geodetic data. Bulletin of the Seismological Society of America 97 (1A), S307–S322, doi:10.1785/0120050632.

Kongko, W., Istiyanto, D. C., Irwandi, I., 2006. Tsunami Modeling and Field Observations of December 26 2004 Indian Ocean Earthquake. Technical Report, Coastal Dynamic Research Center (BPPT), Jogjakarta.

Liew, S. C., Gupta, A., Wong, P. P., Kwoh, L. L., 2010. Recovery from a large tsunami mapped over time: The Aceh Coast, Sumatra. Geomorphology 114, 4, 520-529.

Masselink, G., Hughes, M. G., Knight, J., 2011. Introduction to Coastal Processes and Geomorphology, 2nd edition, Hodder Education, London, pp. 416.

McAdoo, B. G., Paravisini-Gebert, L. (2011). Not the earthquake's fault. Nature Geosciences 4(4), 210-211.

Meilianda, E., Dohmen-Janssen, C., Maathuis, B., Hulscher, S., and Mulder, J., 2010. Short-term morphological responses and developments of Banda Aceh coast, Sumatra Island, Indonesia after the tsunami on 26 December 2004. Marine Geology, 275, 1, 96-109.

Meltzner, A. J., Sieh, K., Abrams, M., Agnew, D. C., Hudnut, K. W., Avouac, J.-P., and Natawidjaja, D. H., 2006. Uplift and subsidence associated with the great Aceh-Andaman earthquake of 2004. Journal of Geophysical Research 111, B02407.

Meltzner, A. J., Sieh, K., Chiang, H. -W., Shen, C. - C., Suwargadi, B. W., Natawidjaja, D. H., Philibosian, B. E., Briggs, R. W. and Galetzka, J. (2010): Coral evidence for earthquake recurrence and an A.D. 1390 - 1455 cluster at the south end of the 2004 Aceh – Andaman rupture, J. Geophys. Res., 115, B10402.

Monecke, K., Finger, W., Klarer, D., Kongko, W., McAdoo, B. G., Moore, A. L., and Sudrajat, S. U., 2008. A 1,000-year sediment record of tsunami recurrence in northern Sumatra. Nature 455, 7217, 1232-1234.

Monecke, K., Templeton, C.T., Finger, W., Houston, B.L., Stefan M Luthi, S. M., McAdoo, B.G., Meilianda, E., Storms, J. E. A., Walstra, D.-J., Amna, R., Hood, N., Karmanocky, F. J., Nurjanah, Rusydy, I., Sudrajat, S. U., 2015. Beach Ridge Patterns in West Aceh, Indonesia, and their Response to Large Earthquakes along the Northern Sunda Trench. Quaternary Science Reviews, Special Issue: Megathrust Earthquakes, 113, 159-170.

Morton, R. A., Goff, J. A., Nichol, S. L., 2008. Hydrodynamical implications of textural trends in sand deposits of the 2004 tsunami in Sri Lanka. Sedimentary Geology 207, 56–64.

Nelson, A.R., Manley, W.F., 1992. Holocene coseismic and aseismic uplift of Isla Mocha, south-central Chile. Quaternary International 15/16, 61-76.

Qiu, Q., Barbot, S., Hill, E., Moore, J. D. P., Feng, L., Ezer, T., 2016. Transient flow in the mantle wedge in the last decade following great earthquakes in the Sumatran subduction zone. American Geophysical Union Fall Meeting Abstracts, 2016AGUFM.G51B1102Q.

Rijn, L.C. van, 1987. Mathematical modeling of morphological processes in the case of suspended sediment transport. Thesis, Department of Fluid Mechanics, Delft University of Technology, Delft, The Netherlands.

Roelvink, D., Reniers, A., Van Dongeren, A., Van Thiel de Vries, J., McCall, R., Lescinski, J., 2009. Modelling storm impacts on beaches, dunes and barrier islands. Coastal Engineering 56, 1133–1152.

Roelvink, J.A., Stive, M. J. F., 1990. Sand transport on the shoreface of the Hoalland coast. Proceedings of the 22nd International Conference on Coastal Engineering. ASCE, Delft, Netherlands, 1909-1921.

Ruessink, B.G., Kuriyama, Y., Reniers, A.J.H.M., Roelvink, J.A., Walstra, D.J.R., 2007. Modeling cross-shore sandbar behavior on the time scale of weeks. Journal of Geophysical Research, 112, F03010.

Ruggiero, P., Walstra, D.J.R., Gelfenbaum, G., van Ormondt, M., 2009. Seasonal-scale nearshore morphological evolution: Field observations and numerical modeling. Coastal Engineering 56, 1153-1172.

Schöne, T., Illigner, J., Manurung, P., Subarya, C., Khafid, Zech, C., Galas, R., 2011. GPS-controlled tide gauges in Indonesia – a German contribution to Indonesia's Tsunami Early Warning System. Natural Hazards and Earth System Sciences 11, 731-740.

Shearer, P., Bürgmann, R., 2010. Lessons Learned from the 2004 Sumatra-Andaman Megathrust Rupture. Annual Review of Earth and Planetary Sciences 38, 1, 103-131.

Spencer, T., Brooks, S. M., Möller I., Evans B. R., 2014. Where Local Matters: Impacts of a Major North Sea Storm Surge, EOS Transactions American Geophysical Union 95(30), 269.

Stive, M. J. F., Aarninkhof, S. G. J., Hamm, L., Hanson, H., Larson, M., Wijnberg, K. M., Nicholls, R. J., Capobianco, M., 2002. Variability of shore and shoreline evolution. Coastal Engineering 47(2), 211-235.

Subarya, C., Chlieh, M., Prawirodirdjo, L., Avouac, J. P., Bock, Y., Sieh, K., Meltzner, A. J., Natawidjaja, D. H., McCaffrey, R., 2006. Plate-boundary deformation associated with the great Sumatra-Andaman earthquake. Nature 440, 7080, 46-51.

Tappin, D. R., Evans, H. M., Jordan, C.J., Richmond, B., Sugawara, D., Goto, K., 2012. Coastal changes in the Sendai area from the impact of the 2011 Tohoku-oki tsunami: Interpretations of time series satellite images, helicopter-borne video footage and field observations. Sedimentary Geology 282, 151–174.

Van der Wegen, M., Roelvink, J.A., 2008. Long-term morphodynamic evolution of a tidal embayment using a two-dimensional, process-based model. Journal of Geophysical Research — Oceans and Atmospheres 113 (C3016).

Vargas, G., Farías, M., Carretier, S., Tassara, A., Baize, S., Melnick, D., 2011. Coastal uplift and tsunami effects asociated to the 2010 Mw 8.8 Maule earthquake in Central Chile. Andean Geology 38 (1), 219-238.

Walstra, D.J.R., 2000. Unibest-TC Userguide. WL | Delft Hydraulics report Z2897.

Walstra, D.J.R., Reniers, A.J.H.M. R., Ranasinghe, J.A. Roelvink, B.G. Ruessink, B.G., 2012. On bar growth and decay during inter-annual net offshore migration. Coastal Engineering 60, 190–200.

Walstra, D.J.R., Wesselman, D.A., van der Deijl, E.C., Ruessink, B.G., 2016. On the intersite variability in inter-annual nearshore sandbar cycles. Journal of Marine Science and Engineering 4(1), 15. doi:10.3390/jmse4010015.

Wang, P., Kirby, J.H., Haber, J.D., Horwitz, M.H., Knorr, P.O., Krock, J.R., 2006. Morphological and sedimentological impacts of Hurricane Ivan and immediate poststorm beach recovery along the Northwestern Florida Barrier-Island Coasts. Journal of Coastal Research 22 (6), 1382-1402.

Wells, A., Goff, J., 2007. Coastal dunes in Westland, New Zealand, provide a record of paleoseismic activity on the Alpine fault. Geology 35, 731-734.

Yu, F., Switzer, A. D., Lau, A. Y. A., Yeung, H. Y. E., Chik, S. W., Chiu, H. C., Huang, Z., Pile, J., 2013. A comparison of the post-storm recovery of two sandy beaches on Hong Kong Island, southern China. Quaternary International 304, 163-175.